Eur. Phys. J. A (2015) **51**: 67
DOI 10.1140/epja/i2015-15067-2

THE EUROPEAN PHYSICAL JOURNAL A

Regular Article – Experimental Physics

Multinucleon photonuclear reactions on ^{209}Bi: Experiment and evaluation

S.S. Belyshev[1], D.M. Filipescu[2], I. Gheoghe[2,3], B.S. Ishkhanov[1,4], V.V. Khankin[4], A.S. Kurilik[1], A.A. Kuznetsov[4], V.N. Orlin[4], N.N. Peskov[4], K.A. Stopani[4,a], O. Tesileanu[2], and V.V. Varlamov[4]

[1] Lomonosov Moscow State University, Department of Physics, Moscow, 119991, Russia
[2] Extreme Light Infrastructure – Nuclear Physics/Horia Hulubei National Institute for R&D in Physics and Nuclear Engineering, Bucharest-Magurele, 077125, Romania
[3] Faculty of Physics, University of Bucharest, Bucharest-Magurele, 077125, Romania
[4] Lomonosov Moscow State University, Skobeltsyn Institute of Nuclear Physics, Moscow, 119991, Russia

Received: 23 January 2015 / Revised: 15 April 2015
Published online: 11 June 2015 –
Communicated by C. Broggini

Abstract. Photon activation technique using bremsstrahlug with end-point energy 55.6 MeV is used to induce photonuclear reactions in a ^{209}Bi target. Absolute yields and integrated cross sections of multiparticle reactions (γ, 2n–6n), (γ, 4n1p), and (γ, 5n1p) are obtained. The results are compared to predictions of statistical models using systematical and microscopic description of photoabsorption and to the result of evaluation of the partial photoneutron reaction cross sections. Based on a comparison with existing experimental photoneutron cross sections and model calculations, we make a conclusion that neutron multiplicity assignment in available photoneutron cross sections on ^{209}Bi can be corrected and evaluated cross sections of (γ, 1n) and (γ, 2n) are obtained that are in an agreement with the obtained experimental results.

1 Introduction

Cross sections of photonuclear reactions find a wide use in fundamental and applied nuclear physics. At sufficiently low energies, photonuclear reactions proceed mainly through formation and subsequent decay of highly collective excitation modes such as the isovector giant dipole resonance (IVGDR), and thus are sensitive to both individual and systematic properties of nuclei. A large amount of data has been collected over the years about the photonuclear reactions and libraries and atlases of reaction cross sections on hundreds of nuclei are available [1–4] and used in such areas as nuclear astrophysics and various applications of photon beams. Model calculations are often used when no reliable measurement of the reaction cross section is available. Especially, multiparticle reactions and reactions with outgoing protons are less thoroughly studied in experiments. It is accepted that the statistical approach is the most adequate for description of cross sections of photonuclear reactions for medium and heavy nuclei. General purpose calculation packages such as TALYS [5], GNASH [6], or the combined model [7] offer a simple way to perform this kind of calculations.

In this work we present the results of measurement of yields of multiparticle photonuclear reactions on ^{209}Bi induced by a bremsstrahlung beam with 55.6 MeV endpoint energy and compare the results with model predictions, evaluated cross sections, and data from other experiments. Bismuth is a suitable subject for this kind of experiment being a natural monoisotope with $Z = 83$ protons and $N = 126$ neutrons, *i.e.* a single $1h_{9/2}$ proton over a doubly magic ^{208}Pb core nucleus. The activation technique allows multiple photonucleon reactions channels to be measured independently and, thus, is a good and inexpensive candidate for this kind of experiment. The earliest photonuclear cross section measurement on ^{209}Bi was made by Miller *et al.* [8], who measured the photoneutron yield reaction cross section $\sigma(\gamma, S\mathrm{n})$ using annihilation photons. Using a similar technique, Harvey *et al.* [9] measured partial photoneutron reaction cross sections (γ, 1n), (γ, 2n), (γ, 3n) as well as the total photoneutron (γ, tot) and the photoneutron yield (γ, Sn) cross sections. The photoneutron yield cross section was obtained in [10] using bremsstrahlung. The photoproton reaction (γ, 1p) was also studied using both bremsstrahlung and virtual photons in [11]. Naik *et al.* [12,13] measured bremsstrahlung-weighted average cross sections of the (γ, 3n) to (γ, 6n) reactions. ^{209}Bi has been a tool to study the application of the direct-semi-direct model to the radiative proton capture. In this connection a number of works on radiative proton capture on ^{208}Pb leading to formation of ^{209}Bi have to be mentioned [14–19].

[a] e-mail: hatta@depni.sinp.msu.ru

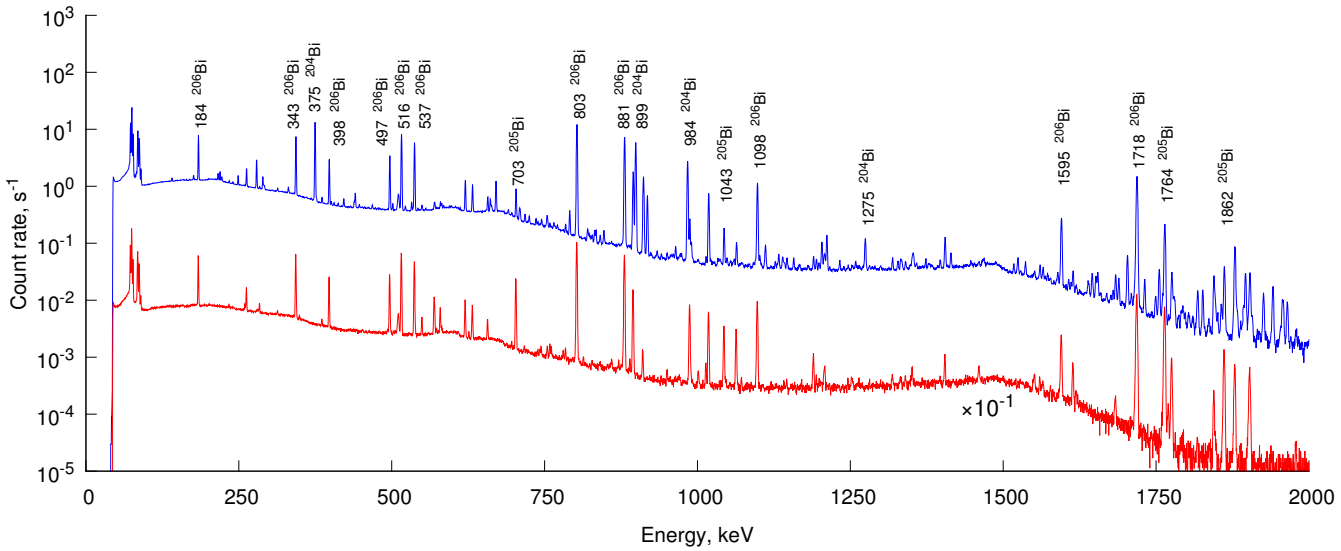

Fig. 1. Two sample spectra of induced gamma-ray activity of the irradiated bismuth target summed over 10 h immediately after the irradiation (upper curve) and 1 week after the irradiation (lower curve, multiplied by 10^{-1}).

2 Experimental technique

The photon activation technique was used to measure yields of photonuclear reactions. The details of the setup and the analysis procedure were described in [20–22]. 55.6 MeV electron beam with the energy spread of about 100 keV, produced by the RTM-55 racetrack microtron [23, 24] of the Skobeltsyn Institute of Nuclear Physics (SINP MSU), struck a 2.1 mm tungsten convertor target and generated a bremsstrahlung beam, which irradiated a 0.83 mm thick bismuth disk 5 cm in diameter. Quick X-ray fluorescence analysis showed that the bismuth target contained at least 99% of ^{209}Bi. For calibration a 0.1 mm copper foil was placed behind the bismuth disk. The irradiation lasted for approximately 30 min, during which the average beam current was 0.24(1) μA (see footnote[1]) as measured by a monitor reaction and an analog-to-digital card connected to the Faraday cup. Three minutes after the irradiation, the bismuth target was moved into the low-background measurement chamber with the Canberra GC3019 high-purity germanium detector (30% relative efficiency, energy resolution of 1.8 keV at 1.332 MeV) to measure the activated spectra. The spectrum acquisition database [21] controlling the InSpector 1250 multi-channel analyzer was used to store gamma-ray spectra of induced activity of the target every 3.5 s for 23 days. The average count rate registered by the detector at 16.5 cm from the target during the first 5 min of the measurement was about 2800 cps.

The obtained gamma-ray spectra were analyzed using the peak fitting module of the spectrum database [22]. Two sample spectra summed over 10 hr starting right after the irradiation and 1 week later are shown in fig. 1.

[1] Throughout the paper we use the computer notation to represent uncertainties: the number in parentheses denotes the error of the last significant digit of a value.

During analysis, the products of the photonuclear reactions were identified by the energies, relative intensities, and half-lives of gamma-lines in the spectra, the corresponding peak areas were determined using least squares fits and, after another fit with exponential decay curves, the corresponding reaction yields were obtained.

We define the reaction yield y as the number of reactions taking place in the target per unit charge of the electron beam, *i.e.* during the irradiation, the number of reaction products n changes according to the following differential equation:

$$\frac{\mathrm{d}n}{\mathrm{d}t} = I_e(t)y - \lambda n(t) + \sum_i k_i\lambda_i n_i(t), \qquad (1)$$

where $I_e(t)$ is the electron beam current and λ is the decay constant. The last term corresponds to accumulation due to decays of other unstable nuclei: λ_i is the decay constant of the i-th parent nucleus and k_i is the branching fraction of the decay. The accumulation was present, *i.e.* this term was non-zero, only for reactions involving proton emission, *i.e.* (γ, 4n1p) and (γ, 5n1p). Without accumulation the solution to the equation is given by

$$n(t) = ye^{-\lambda t}\int_0^t I_e(\tau)e^{\lambda\tau}\,\mathrm{d}\tau, \qquad (2)$$

i.e. the experimental reaction yields can be obtained from the number of decaying product nuclei in the target and from the recorded beam current. In this way, the instability of the electron beam was taken into account.

As said above, the numbers of nuclei n of the reaction products that were used to determine the yields in eq. (2) were calculated from the areas S of the corresponding peaks in the spectra taken at different periods of time after irradiation:

$$n(t) = \frac{S(t, t+T_{\mathrm{real}})}{\varepsilon rc(1-e^{-\lambda T_{\mathrm{real}}})}\frac{T_{\mathrm{real}}}{T_{\mathrm{live}}}, \qquad (3)$$

Table 1. Experimental yields of photonuclear reactions on ^{209}Bi.

Reaction	Product	Half life	J^P	Threshold, MeV	Yield, $10^{10} \times \mathrm{C}^{-1}$	Yield, rel. to 3n
(γ, 2n)	^{207}Bi	31.55 yr	$9/2^-$	14.35	$2.3(2) \cdot 10^4$	7.3(5)
(γ, 3n)	^{206}Bi	6.243 d	6^+	22.44	$3.1(3) \cdot 10^3$	1.0
(γ, 4n)	^{205}Bi	15.31 d	$9/2^-$	29.48	$1.02(8) \cdot 10^3$	0.3308(7)
(γ, 4n1p)	^{204m}Pb	67.2 m	9^-	32.72	4.9(4)	0.00121(6)
(γ, 5n)	^{204}Bi	11.22 h	6^+	37.97	$2.0(2) \cdot 10^2$	0.06490(9)
(γ, 5n1p)	^{203}Pb	52 h	$5/2^-$	41.12	73(7)	0.0235(9)
(γ, 6n)	^{203}Bi	11.76 h	$9/2^-$	45.16	7.8(7)	0.0025(1)

where r is the relative peak intensity, ε is the detector efficiency at the energy of the peak, c is the true coincidence summing correction, λ is the decay constant of the unstable isotope, and $T_{\mathrm{real,live}}$ are, respectively, the total and live time of the spectrum acquisition. In each case the 3.5 second spectra from the spectrum database were combined so as to obtain a reasonable number of points (10–15) over an interval of about five half-lives (where possible). The peak areas in the spectra were determined using least squares, by fitting the spectra with a combination of a Gaussian function and continous background. To correct the peak areas with respect to the true coincidence summing effect, the TrueCoinc [25] program was used. Relative peak intensities of the reaction products were taken from ENSDF [26]. The detector efficiencies were calculated with a calibrated detector model using GEANT4 [27]. For each reaction, the yield was independently calculated from several peaks of the product and the final value was calculated as a weighted average of the obtained results. Yields of only those reactions where the reaction products are unstable were obtained.

The spectra contained peaks from ^{203}Pb and ^{204}Pb, which can be produced both in reactions with outgoing protons and in β-decays of ^{203,204}Bi. In this case, the number of nuclei n was determined in a similar way, except that the last term in eq. (1) was non-zero. The branching fraction of the ^{203}Bi decay into ^{203}Pb is equal to 1.0, and the value for the decay of ^{204}Bi to ^{204m}Pb was calculated from the decay level scheme from [28] $k_{204} = 3.1(3)\%$.

For each reaction product, the most intense and reliably identifiable gamma-lines were used to obtain the yields. The following gamma-lines were used to obtain the yield of ^{207}Bi: 569 keV, 1063 keV, 1770 keV (a small residual activity of ^{207}Bi was detected from the target prior to irradiation, its contribution of about 0.5% was subtracted during analysis; from the 569 keV peak the contribution of ^{205}Bi was subtracted during analysis). Gamma-lines for ^{206}Bi: 537 keV, 803 keV, 881 keV, 1718 keV. For ^{205}Bi: 703 keV, 988 keV, 1043 keV, 1764 keV, 1862 keV. For ^{204}Bi: 375 keV, 899 keV, 984 keV. For ^{203}Bi: 821 keV, 825 keV, 1033 keV. For ^{203}Pb: 279 keV, 401 keV. For ^{204m}Pb: 375 keV, 899 keV, 911 keV, 984 keV (accumulation from ^{204}Bi).

To normalize the reaction yields the total number of initial electrons during the irradiation was obtained from the yield of the $^{65}\mathrm{Cu}(\gamma, 1\mathrm{n})^{64}\mathrm{Cu}$ reaction in the copper monitor target. The evaluated cross section [29] of this reaction was folded with the bremsstrahlung spectrum calculated using a GEANT4 [27] model of the irradiation geometry, giving the reaction yield per one electron. The obtained reaction yields normalized in this way to the total charge of the beam are shown in table 1. It should be noted that the total systematical error affecting the accuracy of the obtained yields is about 10%. About a half of this value is due to the the uncertainty of the position of the irradiated part of the target with respect to the detector and the other part is contributed by the uncertainty of the thickness of the monitor copper foil and the uncertainties of the monitor reaction cross section. Other systematical error sources, such as uncertainties of the relative peak intensities, decay constants and so on contribute less than 1%. Since these factors contribute only as a common multiplier, we also present relative reaction yields, normalized to the (γ, 3n) reaction, where mostly only the statistical errors of the fitted peak areas remain.

3 Model calculations

The obtained experimental yields were compared with theoretical calculations. For this purpose, the model-calculated cross sections $\sigma(E)$ were folded with the bremsstrahlung spectrum at $T = 55.6$ MeV simulated using GEANT4 [27] in the geometry of the experiment,

$$y_{\mathrm{theor}} = \frac{M}{e} \int_0^T \sigma(E)\nu(E,T)\,\mathrm{d}E, \qquad (4)$$

where $\nu(E,T)\mathrm{d}E$ is the bremsstrahlung spectrum, that is, the mean number of photons with energy from E to $E + \mathrm{d}E$ produced by an electron with kinetic energy T, and M is the number of ^{209}Bi nuclei per unit area of the target.

The theoretical cross sections were calculated using two models: TALYS [5], a widely used general purpose nuclear reaction package, and the combined model of photonuclear reactions (CMPNR) [7,30], developed at SINP MSU. Both models are based on the statistical approach and use a combination of the preequilibrium exciton model and particle evaporation process to calculate probabilities of formation of specific final nuclei after absorption of a photon. However, the photon absorption process is

Table 2. Comparison of the experimental yields of photonuclear reactions on ^{209}Bi with model calculations.

Reaction	$10^{10}\times$ Yield, C^{-1}		
	Experiment	CMPNR	TALYS
(γ, p)		$2.58 \cdot 10^3$	66.3
(γ, 2n)	$2.3(2) \cdot 10^4$	$2.53 \cdot 10^4$	$3.01 \cdot 10^4$
(γ, 3n)	$3.1(3) \cdot 10^3$	$2.95 \cdot 10^3$	$3.11 \cdot 10^3$
(γ, 4n)	$1.02(8) \cdot 10^3$	$0.881 \cdot 10^3$	$1.10 \cdot 10^3$
(γ, 4n1p)$_m$	4.9(4)	0.290[a]	0.328
(γ, 5n)	$2.0(2) \cdot 10^2$	$0.750 \cdot 10^2$	$2.29 \cdot 10^2$
(γ, 5n1p)	73(7)	0.421	0.0148
(γ, 6n)	7.8(7)	0.399	6.29

[a] The yield of the ground state of ^{204}Pb has been calculated with the combined model and then multiplied by the isomeric ratio $Y_m/Y_{g.s.}$ from TALYS.

Table 3. Components of photoabsorption cross section on ^{209}Bi calculated using the combined model. E denotes the center of the corresponding Lorentz peak, σ corresponds to its area, $\Gamma_\pi^\uparrow$ is the proton escape width in MeV, $\Gamma_\nu^\uparrow$ is the same for neutrons, $\Gamma^\downarrow$ is the damping (or, spreading) width in MeV, T denotes the isospin splitting branch, and M is the projection of the momentum, corresponding to the deformation branch.

E, MeV	σ, mb	$\Gamma_\pi^\uparrow$	$\Gamma_\nu^\uparrow$	$\Gamma^\downarrow$	T	Type	M
13.63	1262.228	0.001	0.228	3.840	$T_<$	IVGDR	0
32.38	102.065	0.813	1.345	7.307		IVGDR2	
22.76	56.564	0.261	0.720	4.876		IVGQR	0
22.70	112.504	0.258	0.716	4.863		IVGQR	1
22.49	110.456	0.248	0.703	4.822		IVGQR	2
19.93	14.236	0.058	0.000	2.410	$T_>$	IVGDR	
13.38	2524.456	0.000	0.187	3.702	$T_<$	IVGDR	1

described differently. TALYS uses the energy, width, and area of the isovector giant dipole resonance (IVGDR) on ^{209}Bi from the RIPL-3 [31] database, while the combined model uses a microscopic approach to calculate the excitation of the giant dipole and quadrupole resonances and the overtone of IVGDR in deformed nuclear potential, explicitly including the isospin of the excited resonances. In addition, the collective properties of the IVGDR are taken into account at the pre-equilibrium stage. On this basis, in the following discussion we use the photonuclear part of TALYS as an example of a "traditional" statistical model calculation and the combined model as a more microscopic approach, which takes into account those properties of photoexcitation that have the most effect on the cross sections of photonuclear reactions in the energy range spanning from the nucleon separation energy to the mesonic threshold.

The comparison of the experimental yields and the calculations is shown in table 2. In addition the (γ, 1p) reaction, not observed in the experiment, was also included in the comparison. Statistical errors and errors due to determination of the number of target nuclei were about 1% for each calculation. In addition, it is common to estimate the general accuracy of statistical model calculations as about 10–15%.

It is useful to describe the photoabsorption cross section, that is used by both models at the initial stage of calculation. Apart from the quasideutron mechanism cross section which is represented identically by both models using the Levinger parameterization, the photoabsorption cross section in TALYS is represented as a single Lorentz curve with the center at 13.56 MeV, having a peak value of 648 mb, and the width of 3.72 MeV based on the tagged photon measurement [32]. The photoabsorption cross section in the combined model calculation is also a combination of several Lorentz peaks shown in table 3, corresponding to deformation splitting of the giant dipole resonance IVGDR and the giant quadrupole resonance IVGQR (different peaks correspond to different values of the total angular momentum projection M), isospin splitting of the IVGDR (where $T_> = T_0 + 1$ and $T_< = T_0$), and to the $3\hbar\omega$ overtone IVGDR2.

One can see that both theoretical models produce a rather good description of the experimental multi-neutron reaction yields. However, the yields of the reactions with outgoing protons (γ, 4n1p) and (γ, 5n1p) are clearly underestimated by both models and attention is also attracted to a certain discontinuity in the case of (γ, 2n). The observed reaction yield is much lower than the TALYS prediction and is also slightly lower than that of the combined model, which is unexpected since in some cases the agreement is almost exact for the 3n–6n reactions. Further calculation of the (γ, 1n) yields helps to clarify the situation. The combined model gives about $1.75 \cdot 10^{15}\,C^{-1}$, while the result of TALYS is $1.66 \cdot 10^{15}\,C^{-1}$, *i.e.* in the TALYS calculation a fraction of the (γ, 1n) yield flowed into the (γ, 2n) channel. We tend to attribute this behavior to the semi-direct process.

In this discussion of the obtained experimental result, the following basic assumption is made: a photonuclear reaction with outgoing nucleons in the energy region from the nucleon separation threshold to $T = 55.6$ MeV can be classified to one of four mechanisms: direct knockout (DKO), semi-direct, pre-equilibrium, and equilibrium (or evaporation) emission. Of these only the direct knockout mechanism (sometimes called the direct nuclear photoelectric effect) takes place without formation of an intermediate resonance state, while with the others, nucleons are emitted at a certain stage of formation of a collective compound excited state. The contribution of DKO to the proton yield is rather small. The direct proton knockout from ^{209}Bi to excited states of ^{208}Pb has been studied experimentally in [11] at $E_\gamma = 43.7$ and 52.0 MeV, and cross sections of several μb/sr for formation of individual low-lying states of the final nucleus were reported.

In contrast to the pre-equilibrium and evaporation processes, the semi-direct mechanism, or emission of nucleons from the initial 1p1h doorway excitation, depends appreciably on the detailed shell structure of this state. Microscopic models such as direct-semidirect model (DSD) were

used in addition to the statistical model calculations to calculate cross sections of nucleon emission to individual states, *e.g.* (γ, p_0), in [16,33]. A different approach is used in the combined model [7,30], where the semi-direct process is identified with the first stage of the pre-equilibrium process with the exciton number $m = 2$. Instead of using the particle emission rates averaged over all configurations [34,35], the emission rates are calculated as sums of partial rates correspoding to the mixture of single-particle excitations in the initial doorway state.

The result of inclusion of the semi-direct mechanism in the combined model is seen in the calculated yields of (γ, 1n) and (γ, 1p), which are both larger than corresponding "purely statistical" TALYS calculations. The spectra of outgoing neutrons and protons also support this assertion, revealing a large portion of high-energy particles originating from initial stages of the reaction. A related additional effect of the collectivization of doorway states might be also responsible for the somewhat lower yield of (γ, 2n) measured in the experiment and calculated using the combined model. The threshold of this reaction lies very closely to the peak of the giant dipole resonance, where the coherency of the doorway excitation is most prominent, which leads to increased probability of emission of a single higher energy neutron, while the 2n emission is accordingly inhibited.

We now return to the question of multi-neutron reactions. As it is seen from table 2 both models adequately describe the measured yields of photonucleon reactions with 2–4 outgoing neutrons. However, the yields of the (γ, 5n) and (γ, 6n) reactions are reproduced only in the TALYS calculations and the CMPNR model gives significantly underestimated results. The cross sections of the 5n and 6n reactions calculated by CMPNR are shifted by several MeV towards higher energies as compared to the results of TALYS, while their areas, *i.e.* the integrated cross sections, are almost equal in both models. At 55.6 MeV the bremsstrahlung spectrum overlaps the cross sections of (γ, 5n) and (γ, 6n) only partially and the shifts have a very considerable effect on the photoneutron yield estimates. Uncertainties of the high-energy part of the bremsstrahlung spectrum, that was used to calculate the theoretical yields in eq. (4), arising from, *e.g.*, uncertainties of the electron beam shape at the target, could be one of the reasons that contribute to the difference. Another possible explanation is the description of the quasideutron (QD) mechanism of photon absorption, which dominates in this energy region. The doorway state of the pre-equilibrium QD cascade in CMPNR is the 2p2h state of uncorrelated particles and holes, similarly to the approach taken in [36]. However, the QD mechanism assumes a high degree of correlation between the produced holes and, hence, lower number of degrees of freedom of the quasideutron excitation (in this connection Blan [37] has proposed to consider the 2p1h state as a doorway excitation for the QD cascade). If the correllations in the QD channel are not taked into account then the spurious degrees of freedom effectively "consume" some part of the excitation energy which leads to shifts of the multi-nucleon cross sections towards higher energies.

It should be noted that the strength and position of the IVGQR resonance was measured with high precision at the HIγS facility [38], where only about a half of the $E2$ sum rule was found at 23 MeV. This is consistent with the systematics used for the IVGQR in the combined model, and the other part of the strength can be attributed to the low-lying isoscalar quadrupole resonance.

We now consider the reaction yields with a proton in the exit channel, which are both underestimated by model calculations. Although it is tempting to attribute the unusually high observed yields of ^{204m}Pb and ^{203}Pb to a possible admixture of the stable ^{204}Pb isotope in the irradiated target, we could not find a sufficient amount of lead impurities: the upper limit for ^{204}Pb in the bismuth target is 0.01% from X-ray flourescence analysis, and 0.001% from the analysis of the 331 and 361 keV gamma-lines of ^{201}Pb in the spectra, which roughly corresponds to 1–10% of the observed yields. Thus, we think that the observed yield of ^{204m}Pb and ^{203}Pb can not be described by possible impurities in the target, however, a more precise measurement is probably needed for a unambiguous answer.

It is well known that emission of protons in photonuclear reactions on medium and heavy nuclei is often extremely underestimated by statistical models. In the medium mass region a great role is played by the isospin splitting of the IVGDR. However, for heavy nuclei, since the ground state isospin is large ($\frac{43}{2}$ in ^{209}Bi), this effect does not contribute to the photoproton cross section (the probability of excitation of the $T_>$ branch is only about 0.4%). Again, the largest part of photoproton emission in heavy nuclei comes from the semi-direct reaction channel, as shown, *e.g.* for ^{197}Au in [39]. On the other hand, it is likely that this is not the reason of the obtained difference between experimental and calculated yields of the (γ, 4n1p) and (γ, 5n1p) reactions, since the thresholds of these reactions are about 33 and 41 MeV, respectively, and, thus lie far behind the IVGDR. In fact little systematical information is known about photoabsorption at the high-energy tail of the giant dipole resonance and other resonance structures in this region, especially about the emission and spreading decay widths of IVGQR. Clearly, additional tuning of models is required to realistically reproduce multi-nucleon reaction cross sections in this energy region.

Based on the calculations performed using the combined model and the obtained yields we estimated the integrated cross sections from threshold to $T = 55.6$ MeV for those reactions where cross section peaks lie within the energy range of generated bremsstrahlung. $\sigma_{\rm int}(\gamma, 2n) = 7.1(7)$ mb MeV, $\sigma_{\rm int}(\gamma, 3n) = 2.4(2)$ mb MeV, $\sigma_{\rm int}(\gamma, 4n) = 1.7(1)$ mb MeV.

4 Evaluated photoneutron cross sections

4.1 Comparison with experimental (γ, 2n) cross section

The obtained experimental data can be compared with existing previous measurements. The cross sections of

photoneutron reactions on ^{209}Bi were measured in [8–10]. At the Lawrence Livermore National Laboratory (LLNL) Harvey *et al.* [9] used quasimonochromatic annihilation photon beam and a ring-ratio neutron multiplicity sorting method to measure cross sections of partial photoneutron reactions. (γ, 1n) and (γ, 2n) reaction cross sections from this measurement are included in the IAEA compilation of 1999 [1] and are a part of other widely used databases. Since the outgoing protons were not detected, the reported (γ, 2n) cross section is in fact a sum $\sigma(\gamma, 2n) + \sigma(\gamma, 2n1p)$. If the same technique as in the previous section is applied to calculate the corresponding yield for the (γ, 2n) reaction, one obtains the value $y_{\mathrm{LLNL}} = 2.53(7) \cdot 10^{14}\,\mathrm{C}^{-1}$. The LLNL cross section goes only up to 26.4 MeV, and in order to calculate the yield in a 55.6 MeV bremstrahlung spectrum the cross sections was extended into higher energies with the combined-model–calculated theoretical cross section.

4.2 Evaluated cross sections

The y_{LLNL} value significantly exceeds the result of the present measurement, and the difference should not be attributed to the contribution of (γ, 2n1p), which is smaller by about two orders of magnitude. It has been shown in multiple works previously (see [40] and references therein) that the partial photoneutron reaction cross sections measured with neutron detectors often contain errors due to shortcomings of neutron multiplicity sorting. To compensate to some extent the unwanted contribution of wrong multiplicity neutrons, the evaluation of the partial photoneutron reaction cross sections was performed following the procedure described in [40].

The evaluation is based on the observation that many partial photoneutron reaction cross sections, that is the (γ, 1n), (γ, 2n), and (γ, 3n) reactions, measured using direct detection of neutrons at different laboratories, do not agree with each other [40, 41]. It has been suggested that the difference is due to incorrect classification of some of the detected neutrons, where, *e.g.*, a neutron originating from the 1n reaction is assigned to the 2n channel, and vice versa. This kind of errors arises from using the kinetic energy to classify neutrons from different reaction channels, whose energy spectra overlap. For this reason the evaluated partial reaction cross sections are obtained from the photoneutron yield cross section

$$\sigma(\gamma, Sn) = \sigma(\gamma, 1n) + \sigma(\gamma, 1n1p) + 2\sigma(\gamma, 2n) + 2\sigma(\gamma, 2n1p) + \ldots, \quad (5)$$

which is instead a directly measured quantity. The experimental $\sigma(\gamma, Sn)$ cross section is then multiplied by theoretical coefficients

$$F_i^{\mathrm{theor}} = \frac{\sigma^{\mathrm{theor}}(\gamma, in)}{\sigma^{\mathrm{theor}}(\gamma, Sn)}, \quad (6)$$

calculated using the CMPNR model to obtain the evaluated partial photoneutron cross sections.

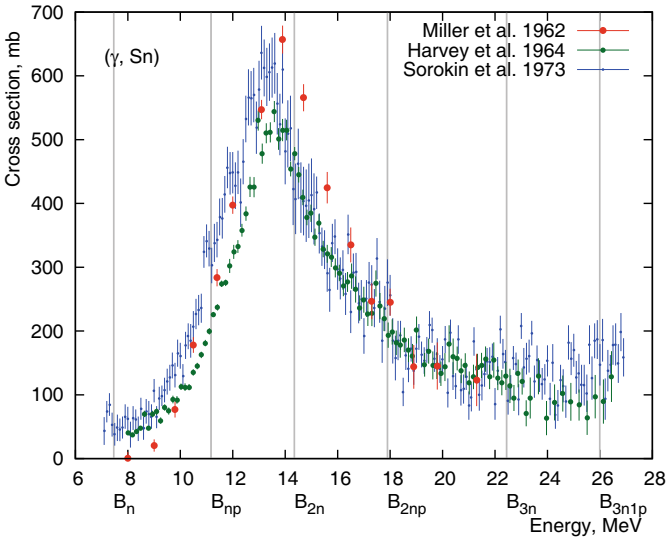

Fig. 2. Photoneutron yield reaction cross sections $\sigma(\gamma, Sn)$ measured by Miller *et al.* [8], Harvey *et al.* [9], and Sorokin *et al.* [10].

Figure 2 illustrates the choice of the $\sigma(\gamma, Sn)$ cross section to be used for the evaluation. The photoneutron yield cross section on ^{209}Bi was measured independently in works [8–10] and is available in the EXFOR database [2–4]. However, the cross section from [8] has a smaller overall number of data points, and the behaviour near threshold is very different as compared to other results. The cross section from [10] has wider error bars and is slightly shifted towards the low energies in comparison to the other two, which might be due to the employed experimental technique. The target had been irradiated with bremsstrahlung at different electron energies, and the obtained reaction yields as a function of energy were unfolded into corresponding cross sections. Uncertainties of the instrument function, *i.e.* in this case the bremsstrahlung spectrum, can lead to energy shifts. Therefore, the Livermore $\sigma(\gamma, Sn)$ from [9] was chosen as a base for the evaluation.

A comparison of the experimental photoneutron yield cross section from [9] to the calculation of the combined model is shown in fig. 3. It is seen that the theoretical cross section calculated using the combined model very closely matches the experimental data points multiplied by a scaling factor 1.12 when slightly shifted by 0.15 MeV towards higher energies. The scaling factor was chosen so as to equalize the area of the experimental and theoretical (γ, Sn) cross section, since the photoneutron yield cross sections measured using the Livermore neutron detector are systematically about 12% lower than corresponding measurements by other groups [40]. Reference [42] recommends a higher value of 1.22, to bring the 1n part of the photoneutron yield to the (γ, 1n) cross section of [32]. However, this scaling results in exaggerated cross section of (γ, 2n) and the 1.12 scaling factor is also more consistent with the data of ref. [10].

This scaled version of the $\sigma(\gamma, Sn)$ cross section was used for multiplication by the F_i coefficients. The

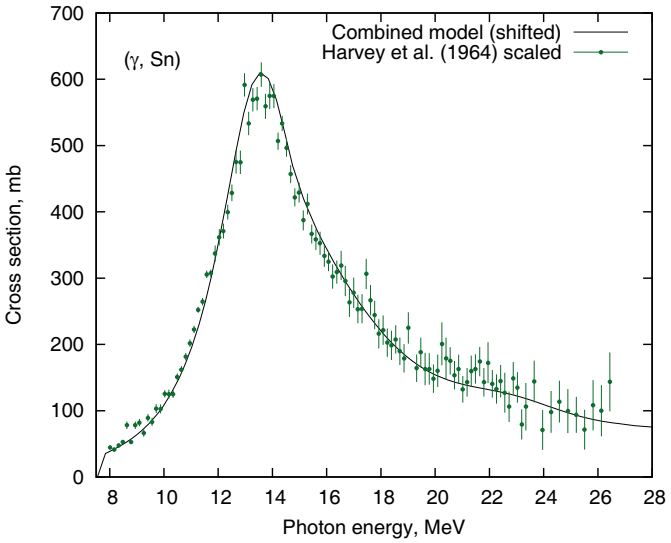

Fig. 3. Photoneutron yield reaction cross section $\sigma(\gamma, S\mathrm{n})$ from [9] scaled by 1.12 and matching of the theoretical cross section to it when shifted by 0.15 MeV.

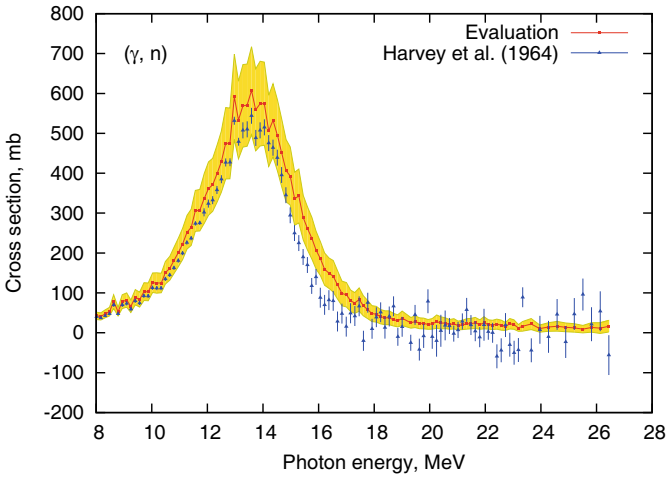

Fig. 4. Evaluated partial photoneutron reaction cross sections $\sigma(\gamma, 1\mathrm{n})$ compared to the experimental cross sections from [9]. The uncertainty of the evaluated cross section is denoted with yellow-filled band.

evaluated partial photoneutron cross sections on ^{209}Bi obtained in this way are shown in figs. 4 and 5. The errors of the evaluation were obtained using interpolation of the experimental errors and the above-made estimate of the accuracy of the model calculations, *i.e.* 10%.

One can see that behind the $B_{2\mathrm{n}}$ threshold the evaluated $\sigma(\gamma, 1\mathrm{n})$ is larger than the experimental cross section, while the $\sigma(\gamma, 2\mathrm{n})$ is correspondingly reduced, *i.e.* some neutrons from the 2n channel were reclassified as coming from the 1n.

The evaluated cross section $\sigma(\gamma, 2\mathrm{n})$ was used to calculate the reaction yield in the activation experiment giving a value $y_{\mathrm{eval}} = 2.43(7) \cdot 10^{14}\,\mathrm{C}^{-1}$. If instead of scaling the Livermore cross section to the model the scaling is done in the inverse direction $y_{\mathrm{eval}} = 2.20(3) \cdot 10^{14}\,\mathrm{C}^{-1}$.

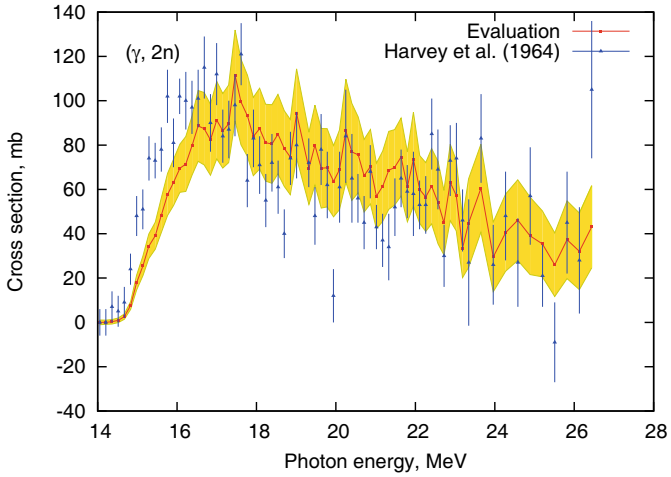

Fig. 5. Evaluated partial photoneutron reaction cross sections $\sigma(\gamma, 2\mathrm{n})$ compared to the experimental cross sections from [9]. The uncertainty of the evaluated cross section is denoted with yellow-filled band.

The choice of the normalizing factor that is used during preparation of the $(\gamma, S\mathrm{n})$ cross section is closely related to the IVGDR enhancement factor κ, that represents the correction to the TRK dipole sum rule arising from the meson exhange currents:

$$\sigma_{\mathrm{int}}(E1) = (1+\kappa)60\frac{NZ}{A}\ \mathrm{MeV\,mb}. \qquad (7)$$

For most medium and heavy nuclei $\kappa \approx 0.3$, however it was suggested on the basis of elastic photon scattering data in [43] that an increased value of 0.46 is more likely for ^{209}Bi due to its shell structure. In [44] this value was re-measured and found to be 0.29, and [45] suggests a value of 0.08. Since the values of κ used in the combined model $\kappa_{\mathrm{c.m.}} = 0.3$ and in TALYS $\kappa_{\mathrm{TALYS}} = 0.26$ lead to a good agreement with the experimental yields, this can be viewed as an evidence against the unusual κ in ^{209}Bi. Combining the yields of $(\gamma, 2\text{–}4\mathrm{n})$ calculated by both models and neglecting the differences of photoabsorption and partial cross sections of both models we can calculate the weighted ratio $\frac{\kappa_{\mathrm{exp}}}{\kappa_{\mathrm{model}}} = 0.97(3)$. However, since the yield of the $(\gamma, 1\mathrm{n})$ reaction, which exhausts most of the photoabsorption cross section, was not measured in this experiment, the obtained result is, thus, only an estimation.

5 Conclusions

Yields of multi-particle photonuclear reactions on ^{209}Bi were obtained using the photon activation technique. The experimental results were analyzed with the help of theoretical models. Integrated cross sections of the $(\gamma, 2\mathrm{n})$, $(\gamma, 3\mathrm{n})$, and $(\gamma, 4\mathrm{n})$ were estimated. The evaluated cross sections of partial photoneutron reactions $(\gamma, 1\mathrm{n})$ and $(\gamma, 2\mathrm{n})$ on ^{209}Bi were produced using the combined model-based approach and experimental $(\gamma, S\mathrm{n})$ cross sections. The obtained evaluation is in agreement with the results

of a photon activation experiment, while the experimental cross section of the $(\gamma, 2n)$ obtained using neutron multiplicity sorting based on the detected kinetic energy is apparently overestimated. Statistical model calculations of this reaction also overestimate photoneutron reactions, and underestimate the reactions with outgoing protons.

The authors are thankful to Prof. H. Utsunomiya (Konan University, Japan) for useful discussions and comments. S.S. Belyshev, B.S. Ishkhanov, V.V. Khankin, A.S. Kurilik, A.A. Kuznetsov, V.N. Orlin, N.N. Peskov, K.A. Stopani and V.V. Varlamov acknowledge partial financial support of the Russian Foundation for Basic Research (project No. 13-02-00124). D.M. Filipescu, O. Tesileanu and I. Gheorghe acknowledge financial support from the Extreme Light Infrastructure Nuclear Physics (ELI-NP) Phase I, a project co-financed by the Romanian Government and the European Union through the European Regional Development Fund (425/12.12.2012, POS CCE, ID 1334 SMIS-CSNR 40741).

References

1. *Handbook of photonuclear data for applications: Cross sections and spectra*, Tech. Rep. IAEA-TECDOC-1178 (IAEA, Vienna, 2000).
2. *Russia Lomonosov Moscow State University Skobeltsyn Institute of Nuclear Physics Centre for Photonuclear Experiments Data database "Nuclear Reaction Database (EXFOR)"*, `http://cdfe.sinp.msu.ru/exfor` (2014).
3. *USA National Nuclear Data Center database "CSISRS and EXFOR Nuclear reaction experimental data"*, `http://www.nndc.bnl.gov/exfor` (2014).
4. *IAEA Nuclear Data Section "Experimental Nuclear Reaction Data (EXFOR)"*, `http://www-nds.iaea.org/exfor` (2014).
5. A. Koning, S. Hilaire, M. Duijvestijn, in *Proceedings of the International Conference on Nuclear Data for Science and Technology - ND2007, May 22 - 27, 2007*, edited by O. Bersillon, F. Gunsing, E. Bauge, R. Jacqmin, S. Leray (EDP Science, Nice, France, 2008) pp. 211–214; see also `http://www.talys.eu`.
6. P.G. Young, E.D. Arthur, M.B. Chadwick, *GNASH, A preequilibrium, statistical nuclear-model code for calculation of cross sections and emission spectra. Report*, Tech. Rep. LA-12343-MS (Los Alamos National Laboratory, 1992).
7. B. Ishkhanov, V. Orlin, Phys. Part. Nucl. **38**, 232 (2007).
8. J. Miller, C. Schuhl, C. Tzara, Nucl. Phys. **32**, 236 (1962).
9. R.R. Harvey, J.T. Caldwell, R.L. Bramblett, S.C. Fultz, Phys. Rev. B **136**, 126 (1964).
10. Y.I. Sorokin, V.A. Khrushchev, B.A. Yuryev, Izv. Akad. Nauk SSSR, Ser. Fiz. **33**, 1891 (1973).
11. D. Branford, A.W. Rauf, J. Lác, J.O. Adler, T. Davinson, D.G. Ireland, C.W. de Jager, M. Liang, W.J. Kasdorp, L. Lapikás, B. Nilsson, H. Ruijter, D. Ryckbosch, A. Sandell, B. Schröder, A.C. Shotter, G. van der Steenhoven, R. Van de Vyver, P.J. Woods, Phys. Rev. C **63**, 014310 (2000).
12. H. Naik, S. Singh, A.V.R. Reddy, V.K. Manchanda, S. Ganesan, D. Raj, M.S. Rahman, K.S. Kim, M.W. Lee, G. Kim, Y.D. Oh, H.-S. Lee, M.-H. Cho, I.S. Ko, W. Namkung, Eur. Phys. J. A **41**, 323 (2009).
13. H. Naik, S. Singh, A. Goswami, V.K. Manchanda, G. Kim, K.S. Kim, M.-W. Lee, M. Shakilur Rahman, D. Raj, S. Ganesan, S. Suryanarayana, M.-H. Cho, W. Namkung, Nucl. Instrum. Methods Phys. Res. B **269**, 1417 (2011).
14. A. Likar, F. Sever, R. Martinčič, Nucl. Phys. A **307**, 77 (1978).
15. A. Likar, T. Vidmar, Nucl. Phys. A **611**, 56 (1996).
16. A. Likar, T. Vidmar, Nucl. Phys. A **593**, 69 (1995).
17. A. Likar, M. Lipoglavšek, M. Vencelj, T. Vidmar, R.A. Bark, E. Gueorguieva, F. Komati, J.J. Lawrie, S.M. Maliage, S.M. Mullins, S.H.T. Murray, T.M. Ramashidzha, Phys. Rev. C **73**, 044609 (2006).
18. K.A. Snover, K. Ebisawa, D.R. Brown, P. Paul, Phys. Rev. Lett. **32**, 317 (1974).
19. K.A. Snover, J.F. Amann, W. Hering, P. Paul, Phys. Lett. B **37**, 29 (1971).
20. S.S. Belyshev, K.A. Stopani, S.Y. Troschiev, A.S. Kurilik, A.A. Kuznetsov, Moscow Univ. Phys. **66**, 363 (2011).
21. S.S. Belyshev, K.A. Stopani, Moscow Univ. Phys. **68**, 88 (2013).
22. S.S. Belyshev, A.N. Ermakov, B.S. Ishkhanov, V.V. Khankin, A.S. Kurilik, A.A. Kuznetsov, V.I. Shvedunov, K.A. Stopani, Nucl. Instrum. Methods Phys. Res. A **745**, 133 (2014).
23. A. Karev, A. Lebedev, V. Raevsky *et al.*, in *Proc. XXII Russian Particle Accelerator Conference RuPAC-2010*, p. 316.
24. A. Ermakov, V. Khankin, N. Pakhomov *et al.*, in *Proc. XXIII Russian Particle Accelerator Conference RuPAC-2012*, p. 538.
25. S. Sudár, in *Specialized software utilities for gamma ray spectrometry, IAEA-TECDOC-1275* (International Atomic Energy Agency, Vienna, Austria, 2002).
26. *Evaluated Nuclear Structure Data File (ENSDF)*, `http://www.nndc.bnl.gov/ensdf/`.
27. S. Agostinelli *et al.*, Nucl. Instrum. Methods Phys. Res. A **506**, 250 (2003).
28. C.J. Chiara, F.G. Kondev, Nucl. Data Sheets **111**, 141 (2010).
29. V. Varlamov, N. Efimkin, B. Ishkhanov, V.V. Sapunenko, M. Stepanov, Bull. Russ. Acad. Sci.: Phys. **59**, 911 (1995).
30. B.S. Ishkhanov, V.N. Orlin, Phys. At. Nucl. **74**, 19 (2011).
31. R. Capote, M. Herman, P. Obložinský, P.G. Young, S. Goriely, T. Belgya, A.V. Ignatyuk, A.J. Koning, S. Hilaire, V.A. Plujko, M. Avrigeanu, O. Bersillon, M.B. Chadwick, T. Fukahori, Z. Ge, Y. Han, S. Kailas, J. Kopecky, V.M. Maslov, G. Reffo, M. Sin, E.S. Soukhovitskii, P. Talou, Nucl. Data Sheets **110**, 3107 (2009).
32. L.M. Young, *Photoneutron cross-sections and spectra from monoenergetic photons on yttrium, praseodymium, lead, and bismuth in the giant-resonance*, PhD thesis, University of Illinois at Urbana-Champaign (1972).
33. E. Běták, A. Likar, T. Vidmar, *Radiative nucleon capture - a dual approach*, in *Proceedings of the International Conference on Nuclear Data for Science and Technology, April 22-27, 2007, Nice, France*, edited by O. Bersillon, F. Gunsing, E. Bauge, R. Jacqmin, S. Leray (EDP Sciences, 2008) pp. 191–194.
34. J. Dobeš, E. Běták, Z. Phys. A **310**, 329 (1983).
35. C. Cline, M. Blann, Nucl. Phys. A **172**, 225 (1971).
36. J.R. Wu, C.C. Chang, Phys. Rev. C **16**, 1812 (1977).
37. M. Blann, B.L. Berman, T.T. Komoto, Phys. Rev. C **28**, 2286 (1983).

38. S.S. Henshaw, M.W. Ahmed, G. Feldman, A.M. Nathan, H.R. Weller, Phys. Rev. Lett. **107**, 222501 (2011).
39. T. Tamae, T. Hino, H. Kawahara, M. Nomura, M. Sugawara, A. Tanaka, T. Tanaka, H. Tsubota, T. Yokokawa, T.K. Yoshida, Nucl. Phys. A **690**, 355 (2001).
40. V.V. Varlamov, B.S. Ishkhanov, V.N. Orlin, K.A. Stopani, Eur. Phys. J. A **50**, 114 (2014).
41. E. Wolynec, A.R.V. Martinez, P. Gouffon, Y. Miyao, V.A. Serrão, M.N. Martins, Phys. Rev. C **29**, 1137 (1984).
42. B. Berman, R. Pywell, S. Dietrich, M. Thompson, K. McNeill, J. Jury, Phys. Rev. C **36**, 1286 (1987).
43. R. Nolte, F. Schröder, A. Baumann, K. Rose, K. Fuhrberg, M. Schumacher, P. Fettweis, R. Carchon, Phys. Rev. C **40**, 1175 (1989).
44. D.S. Dale, A.M. Nathan, F.J. Federspiel, S.D. Hoblit, J. Hughes, D. Wells, Phys. Lett. B **214**, 329 (1988).
45. S. Kahane, Phys. Rev. C **33**, 1793 (1986).